

# Find the Fruit: Designing a Zero-Shot Sim2Real Deep RL Planner for Occlusion Aware Plant Manipulation

**Nitesh Subedi\***

Department of Mechanical Engineering  
Iowa State University, United States  
nitesh@iastate.edu

**Hsin-Jung Yang\***

Department of Mechanical Engineering  
Iowa State University, United States  
hji@iastate.edu

**Devesh K. Jha**

Mitsubishi Electric Research Laboratories  
United States  
jha@merl.com

**Soumik Sarkar**

Department of Mechanical Engineering  
Iowa State University, United States  
soumiks@iastate.edu

*\*Equal Contribution*

**Abstract:** This paper presents an end-to-end deep reinforcement learning (RL) framework for occlusion-aware robotic manipulation in cluttered plant environments. Our approach enables a robot to interact with a deformable plant to reveal hidden objects of interest, such as fruits, using multimodal observations. We decouple the kinematic planning problem from robot control to simplify zero-shot sim2real transfer for the trained policy. Our results demonstrate that the trained policy, deployed using our framework, achieves up to 86.7% success in real-world trials across diverse initial conditions. Our findings pave the way toward autonomous, perception-driven agricultural robots that intelligently interact with complex foliage plants to “find the fruit” in challenging occluded scenarios, without the need for explicitly designed geometric and dynamic models of every plant scenario.

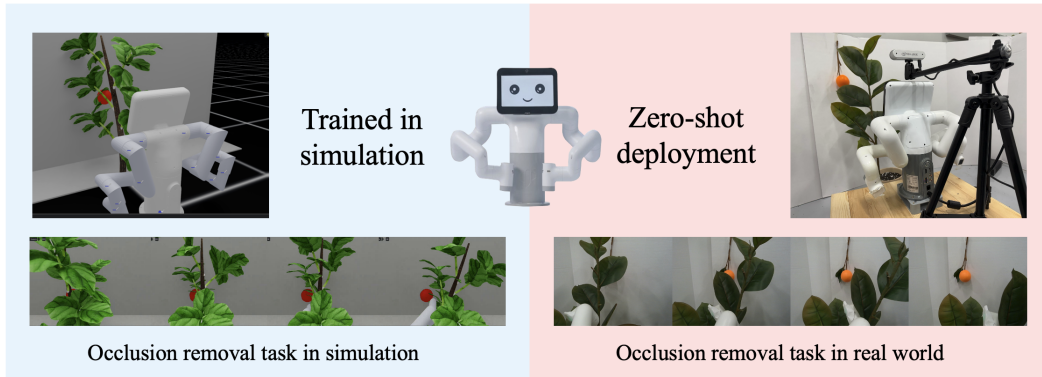


**Figure 1: Top:** End-to-end RL training on a generic deformable plant in simulation (left), with the learned policy deployed zero-shot on a real stemmed plant (right) using the MyBuddy 280 robot (center). **Bottom:** Frame-by-frame sequences of occlusion removal in simulation (left) and real-world trials (right), showing that the policy trained on an abstract model generalizes to experimental plants.

**Keywords:** Reinforcement Learning, Sim2real Transfer, Zero-Shot Transfer, Deformable Object Manipulation

## 1 Introduction

In general, robotic systems achieve robust performance in domains where environmental conditions are inherently more structured and predictable. Applications such as manufacturing [1, 2, 3] and

laboratory automation [4, 5] demonstrate how advances in perception and control have enabled consistent, precise manipulation when tasks are well-defined and variability is limited. However, many real-world domains, particularly those with dynamic, cluttered, and deformable objects, present greater challenges. Agricultural harvesting is a representative example of such. In these environments, target objects are frequently occluded by dense, flexible structures that must be actively manipulated to enable access. Prior work has attempted to address this challenge by manipulating plant branches without visual feedback [6] or relying instead on preplanned configurations [7]. Without real-time sensory guidance, such strategies often lead to inefficient fruit searching. Other efforts favor minimal-contact interaction [8, 9], where robots avoid direct manipulation of foliage and rely on delicate grasping. Such approaches typically reduces effectiveness in dense, highly occluded environments. The limitations highlight the need for adaptive, vision-guided, occlusion-aware manipulation strategies capable of interacting with complex, deformable plant structures.

Interaction with deformable materials such as plant structures introduces additional complexity. Unlike rigid objects, flexible bodies deflect in dynamic and often unpredictable ways, making predicting the outcome of a given action difficult. Each deformation alters the scene’s geometry, contact forces, and the robot’s perceptual inputs, complicating both planning and real-time decision-making. Research on deformable object manipulation in robotics has primarily focused on simpler objects or structured approaches. For example, there are works on rope/chain manipulation [10, 11, 12], fabrics [13, 14, 15, 16], and soft tissues handling [17] using model-based or learning-based methods. In agricultural robotics, progress has been fragmented. Some methods focus on removing individual leaves obstructing a known target [18, 19]; others use self-supervised learning to predict the space revealed by a given action, enabling multi-step exploration of occluded regions [20]. Branch manipulation and obstacle repositioning before harvesting have also been studied [21, 22], as have carefully planned, collision-free grasping strategies that assume fruits are already detected [23, 24]. Many of these approaches depend on explicit detection of plant parts or precise 3D scene reconstruction [25, 26, 27], which limits scalability in cluttered, dynamic field environments due to computational complexity and the difficulty of modeling deformable structures. In contrast, an end-to-end learned policy, if trained and transferred successfully, could handle occlusions reactively and adaptively without relying on brittle intermediate representations.

Reinforcement learning (RL) with simulation offers a promising alternative by enabling agents to acquire adaptive behaviors directly through interaction with the simulation environment, without requiring explicit geometric or physical models. However, successfully applying RL in these settings remains a challenge: First, standard RL agents often struggle when interacting with highly deformable objects or operating under dynamic occlusions [28, 29, 30]. Second, policies trained exclusively in simulation using sensor data could be sensitive to discrepancies in perceptual and mechanical properties between simulated and real environments, making sim2real transfer difficult [31, 32, 33]. Please refer to table 1 for a summary of relevant works.

To address these challenges, we propose an end-to-end RL framework for occlusion-aware manipulation of deformable plants with zero-shot sim2real transfer capabilities. The policy is trained entirely in simulation using a manually constructed generic plant model, comprising a central stem and flexible branches, within NVIDIA Isaac Lab [34]. Deformable dynamics and randomized occlusion patterns are introduced to expose the agent to diverse scenarios during training. A Proximal Policy Optimization (PPO) agent [35] learns a control policy through direct interaction with this simulated environment. To enable transfer to physical systems without fine-tuning, we combine extensive domain randomization with an impedance-controlled compliance layer, which decouples high-level motion planning from uncertain contact dynamics. This approach maintains policy robustness even when real plants differ in stiffness, mass distribution from the simulated model. Our contributions are as follows:

1. **End-to-end RL for occlusion-aware plant manipulation:** We present, to our knowledge, the first RL-based system that learns to push aside occluding plant structure and reveal hidden fruit targets autonomously. The policy uses sensory inputs and does not rely on

explicit detection or geometric modeling of every plant part, instead learning an occlusion-resolving behavior from experience.

2. **Zero-shot Sim2real transfer via decoupled kinematics and control:** Using a compliant impedance control scheme, our method achieves zero-shot sim2real transfer without fine-tuning. RL learns the robot’s kinematics, while the low-level controller handles force mechanics, adapting to variations in plant stiffness or mass.

Through this multi-pronged approach, we enable adaptive behaviors that resolve visual occlusions through interaction with flexible plant matter, paving the way for scalable agricultural automation in unstructured environments. Experimental validation shows that our framework achieves upto 86.7% occlusion-resolution success rate in physical trials, a modest drop from 96.1% in simulation, using a generic plant model rather than an exact digital twin. This success highlights the ability of our policy to exploit structural cues, such as a vertical stem, and generalize across individuals of the same morphological class. By advancing the interplay between adaptive perception and compliant control, our findings demonstrate the potential of carefully designed end-to-end RL systems to bridge the gap between laboratory training and deployment in complex real-world agricultural settings.

Literature	Goal	No Recons.	Visual Servo.	RL
Jacob et al. [6]	Reach task	✓	✗	✓
Rijal et al. [7]	Branch manipulation	✗	✓	✗
Zhang and Gupta [20]	Explore occluded regions	✓	✗	✗
Yao et al. [18]	Leaf-occlusion removal	✗	✓	✗
Jenkins and Kantor [26]	Stalk detection	✗	✓	✗
<b>Our work</b>	Adaptive deformable manipulation	✓	✓	✓

**Table 1:** Comparison of representative approaches in agricultural or deformable manipulation. “No Recons.” indicates no use of explicit 3D reconstruction or geometric modeling; “Visual Servo.” denotes visual servoing; “RL” refers to reinforcement learning.

## 2 Preliminaries

### 2.1 Reinforcement Learning

Reinforcement Learning (RL) is a framework where an agent learns to make sequential decisions by interacting with an environment, typically modeled as a Markov Decision Process (MDP)  $(S, A, P, R, \gamma)$ . Here,  $S$  and  $A$  are the state and action spaces,  $P(s'|s, a)$  defines transition dynamics,  $R(s, a, s')$  assigns rewards, and  $\gamma \in [0, 1]$  is the discount factor. At each step  $t$ , the agent observes a state  $s_t$  and selects an action  $a_t \sim \pi(a_t|s_t)$  according to a policy  $\pi_{theta}$ , which is typically parameterized by a neural network  $\theta$ . The agent receives a reward  $r_t$  and transitions to the next state  $s_{t+1} \sim P(\cdot|s_t, a_t)$ . The goal is to maximize the expected discounted return  $R_t = \sum_{k=t}^T \gamma^{k-t} r_k$ .

## 3 Methodology

Our framework integrates perception and control to enable a robot to manipulate deformable plants while resolving occlusions. The approach consists of several components, which we detail below.

### 3.1 Decoupling High-Level Motion Planning and Low-Level Actuation

Manipulating a plant involves contact dynamics between the robot and flexible branches. We adopt a hierarchical control strategy to handle these interactions that decouples high-level planning from low-level actuation. The RL policy operates at the kinematic level, outputting desired incremental joint angles. These are sent to a low-level impedance controller (via servo position control with current limits), which executes motion while enforcing torque bounds. The RL agent plans in configuration space to reduce occlusion, and the controller follows its output. Fig. 2(a) illustrates this

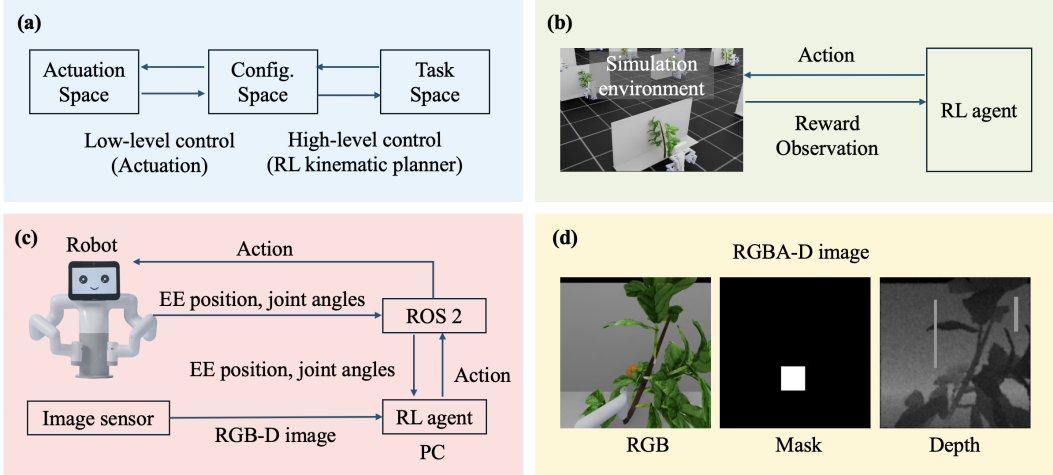


**Figure 2:** (a) Control-space abstraction. The low-level controller implements servo-position control, while the RL agent plans in a higher-level Configuration-Task Space, outputting kinematic commands to achieve task goals. (b) Simulation training loop. The RL agent receives multimodal state observations from the simulation environment and issues continuous action commands. (c) Real-world deployment architecture. An RGB-D sensor streams images to the RL agent running on a PC; the agent’s action outputs are transmitted via ROS 2 to the robot, which executes them and feeds back its current end-effector position and joint angles for closed-loop control. (d) Example of an input observation: RGB channels capture appearance, the depth (D) channel encodes geometry, and the alpha (A) channel provides ground-truth binary mask of the target during training to accelerate learning.

decoupling: the policy acts as a kinematic planner, while the embedded controller handles actuation by applying currents to reach the configuration. This separation has a significant benefit: it improves generalization to unknown plant properties. The policy does not need a perfect model of the plant’s physics, since it never directly computes forces. Instead, we randomize the plant’s physical parameters during training and include torque limits in the simulation to mimic the real behavior. The RL agent thus learns strategies that work under a wide range of effective stiffness conditions.

### 3.2 Reinforcement Learning Problem Formulation

We detail the MDP setup for training the RL policy, including state, action, and reward design.

**State:** The agent’s observation at time  $t$  is a composite of multimodal sensory inputs and proprioceptive data. Each state  $s_t$  includes an RGBA-D image ( $I_{\text{RGBA-D},t}$ , RGB image, alpha fruit mask, depth), joint angles for the waist ( $J_{b,t}$ ) and the left arm ( $J_{i,t}$ , where  $i = 1 \sim 5$ , representing the different joints), and end-effector position ( $EE_{\text{pos},t}$ ). It can be formally represented as  $s_t = [I_{\text{RGBA-D},t}, J_{b,t}, J_{i,t}, EE_{\text{pos},t}]$

**Action:** Actions  $a_t = [\Delta j_{1-5}, \Delta j_b]$  are delta joint angles for the same joints, clipped to  $[-1, 1]$  and scaled at runtime.

**Reward:** The total reward  $r_t$  is a weighted sum of:

- Self-collision penalty,  $r_{sc} = -5$  if collision; 0 otherwise.
- Occlusion reward,  $r_{occ} = (1 - \text{occluded} / \text{fruit pixels}) \times k$ , where  $k$  is a scaling constant controlling the occlusion reward.
- Full visibility reward,  $r_{fv} = 3$ , upon satisfying the success criterion for 1 timestep (Section 3.4).
- Sustained visibility,  $r_{sus} = r_{sv}$  if full visibility is maintained  $\geq 10$  steps; 0 otherwise.
- Post-visibility penalty,  $r_{pv} = \text{mask} \times \text{action magnitude}$ , penalizes post-visibility motion.

These reward terms work in tandem to guide the agent: it gets steady positive feedback as the fruit becomes less occluded, a significant positive signal for complete success, and negative feedback for extraneous actions. By the end of training, the agent learns behaviors that move the plant’s stem to reveal the fruit and then stop, aligning with the behavior needed for our task design.

### 3.3 Simulation Environment Setup

The simulation environment, as shown in Fig. 2(b) is developed using Isaac Lab from NVIDIA Omniverse, ensuring high-fidelity replication of the physical setup. The MyBuddy 280 robot is imported as an URDF model derived from SolidWorks, with joint positions controlled to mirror the behavior of the physical robot closely. Artificial plants are modeled as OBJ meshes converted into deformable bodies using Isaac Lab’s API. Primitive shapes like spheres and cubes were randomly placed behind the plant to mimic the variable fruit location. Domain randomization is applied to improve robustness, including 360° variations in plant orientation and perturbed lighting conditions. The PhysX engine operates at a 1/60 s timestep with eight solver iterations. A white wall is placed behind the fruits to minimize background distractions. All simulations are conducted in Isaac Lab 1.4.0 with an NVIDIA GeForce RTX 4090 GPU (24GB).

### 3.4 Evaluation Metrics

To assess the RL agent’s performance, we define the following evaluation metrics: **(a)** Success rate: the percentage of trials in which at least 90% of the fruit is evident for more than 10 timesteps. **(b)** Steps to goal: The number of steps required to achieve the visibility objective. **(c)** Generalization: The percentage of successful trials across various configurations and environmental setups.

### 3.5 Training and Evaluation of the RL Agent

**Training** We train the policy using PPO [35] from skrl [36] in simulation (Appendix 8), enabling agent to learn continuous control of the robot’s 6-DOF arm. Each episode begins with a randomized robot configuration and fruit location, requiring the agent to adapt to varying viewpoints and occlusion. To promote generalization, we apply domain randomization over physical properties (torque), visual conditions (lighting, textures), and sensor noise. These variations prevent overfitting to a specific environment and bolster robustness to real-world deployment.

To facilitate more efficient learning, we provide the agent with privileged information during training: a ground-truth binary mask highlighting the fruit’s location. This auxiliary input guides the agent toward identifying the fruit earlier, especially when it is heavily occluded, and accelerates the acquisition of effective behaviors. Importantly, the mask is used only during training; at evaluation and deployment, the policy relies solely on sensory observations (see Section 5.2).

After approximately 50 million simulation steps, the agent converges to a policy that reliably finds and exposes fruit by strategically interacting with the plant. Rather than memorizing specific geometry (since the simulation is only an approximation), it learns a general strategy: locate the stem and fruit, move the end-effector along the stem, and push aside occluding structure until the fruit becomes visible. This behavior, shaped by training in diverse randomized environments, generalizes well to real plants with similar stems and occlusion patterns.

**Evaluation** During post-training evaluation in simulation (20,000 randomized episodes mirroring training conditions), the RL agent achieved an overall success rate of **96.09%** (see Appendix Fig. 6 for the plots). In most trials, the agent revealed the fruit with minimal occlusion, demonstrating the robustness and effectiveness of the learned policy. The agent also exhibited efficient behavior, requiring as few as 200 control steps in the easiest scenarios and up to 600 in the most challenging ones (mean episode length:  $\approx$  500 steps). This range indicates adaptability and consistency: even from unfavorable starting positions or highly occluded setups, the policy reliably finds a sequence of actions to achieve visibility.

### 3.6 Deployment Framework

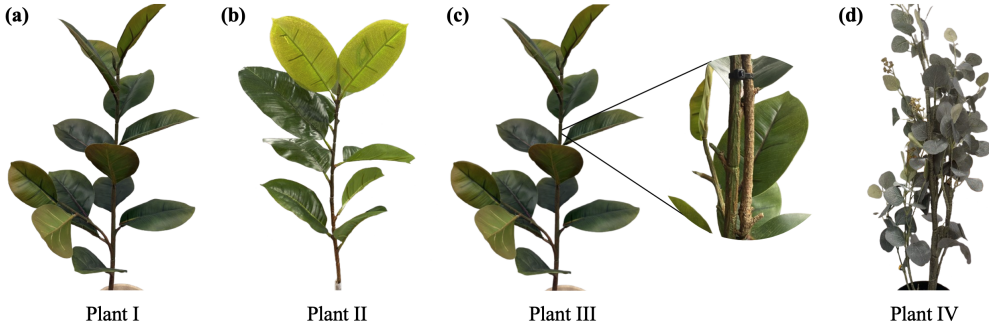
The deployment framework, as shown in Fig. 2(b), integrates the trained RL controller with a low-level servo position controller. The end-effector pose and joint angles are published to ROS 2, where they are subscribed to by the control PC. Simultaneously, an RGB-D image is captured from the

image sensor. These observations are fed into the policy, which subsequently generates an action. The resulting action, converted to the target joint angles, is then published and subscribed to by the robot. At this stage, only kinematic control is involved. To ensure plant safety, a maximum current limit is set for each servo motor, restricting the torque such that it remains insufficient to cause harm. Consequently, the servo position controller attempts to reach the target position in a controlled manner without exerting excessive force on the plant. This process operates in a continuous loop, maintaining safe and effective control.

## 4 Experiments

After training exclusively in simulation, we deployed the policy zero-shot on a physical setup (Fig. 1, top) consisting of a 6-DoF MyBuddy arm, a RealSense camera [37], and a selection of potted, off-the-shelf artificial plants. Camera height, distance, and tilt as well as the plant’s base pose-were fixed to mirror the simulation.

To evaluate generalization, we conducted experiments across a structured grid of initial conditions. Four plant instances, presented in Fig. 3, were considered: two morphologically similar plants, a structurally reinforced variant of one of the former two with increased stiffness, and a visually distinct, bushy plant with the stiffest stem. Each plant exhibits unique stiffness characteristics, enabling evaluation of the policy’s robustness across diverse physical and visual conditions. For each plant, the fruit was placed at nine discrete locations, arranged in a  $3 \times 3$  lattice spanning left/center/right and low/mid/high positions, 20 cm behind the plant (Fig. 4 (a)). The robotic arm was initialized from five pre-selected, self-collision-free joint configurations (Fig. 4 (b)), resulting in  $4 \times 9 \times 5 = 180$  unique trials. In each trial, the arm was reset to its designated pose, the fruit positioned at the target grid cell, and the trained policy was executed for up to 600 control steps at a frequency of 1 Hz, subject to impedance constraints. A trial was considered successful if the robot achieved at least 90% fruit visibility for five consecutive frames. The number of control steps required to achieve success was also recorded.



**Figure 3:** Representative plant instances used for real-world experiments. (a) and (b) show plants with a clearly visible central stem and broad foliage, similar to the simulated morphology. (c) shows a reinforced version of (a), with a mechanically stiffened stem. The zoom-in highlights the reinforcement detail. (d) depicts a dense, bushy plant lacking a distinct central stem, presenting a more severe occlusion challenge. All four plants have different structural stiffness. Together, these variations enable testing of the policy’s robustness across a range of plant geometry and mechanical properties. All plants are artificial.

## 5 Results

### 5.1 Generalization and Failure Mode

**Policy behavior and performance** Fig. 4(c) and (d) summarizes the performance of the trained policy across 180 real-world episodes involving four distinct plant types and multiple fruit locations. Based on initial observations, the robot inferred the likely location of the fruit and anticipated occlusions. The policy then guided the end-effector toward the occluded regions, using compliant motions to maneuver around or near the vertical stem, often pushing it aside. Through training, the

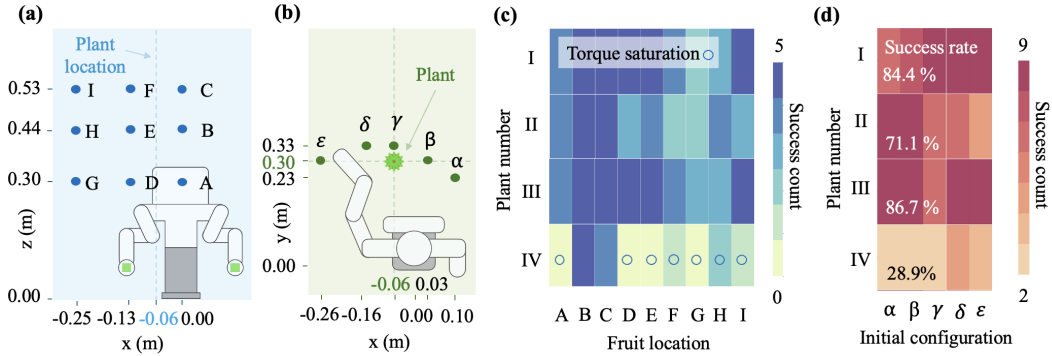


**Figure 4:** (a) Experimental setup showing predefined fruit locations relative to the robot and the plant, viewed from the rear of the robot ( $x$ - $z$  plane). (b) Top-down view ( $x$ - $y$  plane) of the five different initial configurations, presented in end-effector positions. (c) Heatmap of successful trials across all plants (I-IV) and fruit locations (A-I), where success count represents the number of successful attempts out of five trials for each initial configuration. (d) Heatmap of successful trials across all plant (I-IV) and initial configurations ( $\alpha$ - $\epsilon$ ), where success count represents the number of successful attempts out of nine trials for each fruit location. The percentage numbers at the lower left are the success rates across each plant.

policy implicitly learned to treat the stem as a leveraging structure, a consistent physical anchor for manipulation, enabling adaptation across plant configurations. Once sufficient fruit visibility was achieved, the robot typically ceased movement, completing the exposure task. The policy achieved high success rates on Plant I (84.4%), Plant II (71.1%), and Plant III (86.7%), demonstrating robust generalization across mechanical properties of plants. However, performance dropped significantly on Plant IV (28.9%), which presented a visually and mechanically out-of-distribution challenge due to its bushy structure, lack of a visible central stem, and increased stiffness.

**Failure analysis** Upon inspection, we found that the dominant failure mode on Plant IV was due to physical resistance: the robot frequently saturated its motor torque limits, preventing it from reaching the configurations determined by the policy. Notably, in trials that failed, the policy still achieved approximately 70-80% fruit exposure, just below the 90% success threshold, indicating purposeful behavior that could not be fully executed within the torque and time constraints. To further assess the generalization capability under more manageable conditions, we created Plant V, a modified version of Plant IV such that it is more mechanically compliant while preserving its overall structure and visual complexity (see Fig.5(a)) and perform the same tests on it. We focused our evaluation on fruit locations other than G, H, and I, as the softened plant’s foliage was insufficient to meaningfully occlude targets in those areas. As shown in Fig.5(b), the policy achieved an 80% success rate at these locations, matching performance levels observed on Plants I-III. (Note that, the torque still maxes out for all tests for fruit location D, if we include the results from this location, the success rate is 67%). These findings suggest that the learned policy generalizes effectively even to visually distinct plants, as long as mechanical resistance remains within the robot’s actuation limits. For complete results on which exact plant location and configuration failed instead of a success count, please see Appendix Figs. 7-9, and Tables 2-4. In addition, we observed that reduced performance on Plant II, despite its visual similarity to Plant I, stemmed from a perception artifact. Specifically, RealSense depth images for Plant II often produced ghosted or duplicated stem features. This resulted in the policy receiving ambiguous depth cues, leading to occasional misinterpretation of the scene structure. These findings reinforce that the policy generalizes well across morphology, but its success also depends on the fidelity of visual input and the physical executability of its actions. Please refer to Appendix Figs. 12–15 for RGB and corresponding depth images of each plant.

## 5.2 Ablation Study

We conducted two ablation studies to understand better which components are critical for training efficiency and sim2real transfer performance.

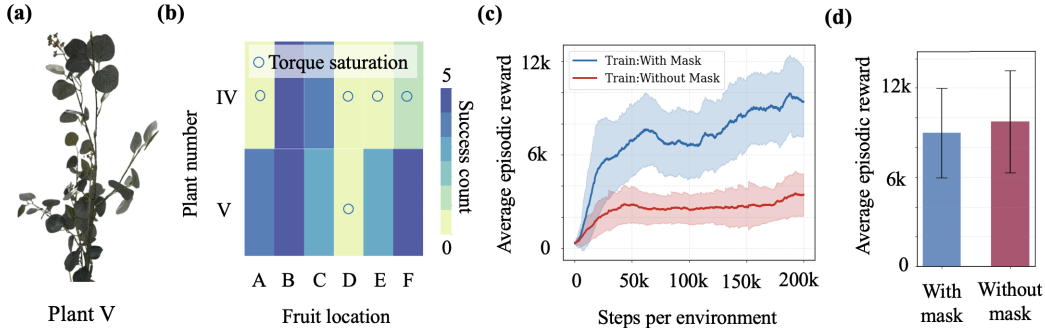


**Figure 5:** (a) The modified version of Plant IV: mechanically more compliant while preserving its overall structure and visual complexity (b) Heatmap of successful trials between Plant IV and V and fruit locations (A-F), where success count represents the number of successful attempts out of five trials for each initial configuration. (c) Training performance with and without access to the ground-truth fruit mask. The mask accelerates learning and improves final returns (d) Evaluation results when deploying the policy trained with the mask: performance remains consistent even when the mask is removed at test time

**Privileged fruit mask during training** Although the deployed policy receives no fruit mask (i.e., an all-zero channel), we optionally provide a ground-truth binary mask from the simulator during training to accelerate learning (as noted in Section 3.5). To evaluate this, we trained two policies under identical conditions—one with the mask included as an input channel, and one without. As shown in Fig. 5 (c) and (d), the policy trained with the mask converged significantly faster and achieved higher returns throughout training. However, after convergence, removing the mask at inference time had minimal impact on performance. This indicates that the mask acts as a privileged learning signal, helping the agent localize the fruit earlier in training, while ultimately encouraging reliance on visual and geometric cues alone. The ablation validates this training-time simplification and confirms that the learned behavior generalizes without the mask at test time.

**Simulation fidelity and visual realism** To evaluate the importance of simulation fidelity, we trained policies in two versions of our environment: (i) a high-fidelity setting with photorealistic textures and realistic lighting, and (ii) a reduced-fidelity variant featuring flat textures and simplified illumination. The policy trained in the high-fidelity simulator transferred successfully to the real-world setting, achieving a success rate upto 86.7%. In contrast, the low-fidelity policy exhibited erratic and unstructured behavior due to a significant visual domain gap, rendering it unsuitable for deployment. The agent failed to generalize basic manipulation behaviors, and as a result, no real-world experiments could be conducted with this policy. These results underscore the critical role of visual realism in enabling effective sim2real transfer, particularly in tasks that rely heavily on visual cues (see Appendix Fig. 11 for the training plot in this setting).

Our results show that an occlusion-aware policy trained on a generic simulated plant can transfer zero-shot to real plants. Without requiring exact digital twins, the simulation’s abstract morphology sufficed to encode structural priors. While precise reconstructions could improve edge-case performance, our approach generalizes across plant instances and morphologies, enabling scalable, perception-driven manipulation in real-world agriculture.

## 6 Conclusion

We presented a deep RL pipeline for occlusion-aware fruit localization and plant manipulation, trained entirely in simulation and deployed zero-shot to real plants. The learned policy uses RGB-D and proprioceptive inputs to uncover occluded fruits by physically interacting with foliage—leveraging the stem as a stable structural cue to guide safe, targeted motion. By decoupling high-level kinematics from low-level dynamics and applying domain randomization, the agent generalizes across diverse conditions without requiring additional fine-tuning. Our approach achieved up to 86.7% success on real stemmed plants using only an abstract, simulated morphology—without relying on exact digital twins. This demonstrates that a structurally representative model with a central

stem and occluding leaves is sufficient to enable robust sim-to-real transfer. While more detailed reconstruction could help in edge cases involving ambiguous geometry or high physical resistance, it is not a prerequisite for effective deployment. These results highlight a promising direction for scalable, perception-driven agricultural robotics that can operate in cluttered, variable environments with minimal task-specific engineering.

## 7 Limitations

While our approach demonstrates strong performance in both simulation and real-world deployment, several limitations define its current scope and point toward valuable directions for future work.

**Simplified training setup.** The policy is trained in a minimal, high-fidelity environment with a single fruit occluded by a generic, single-stem plant. While this abstraction enables robust sim-to-real transfer to morphologically similar plants, it limits exposure to more complex scenarios-such as multi-branch architectures, overlapping fruits. Expanding the simulation environment to support diverse morphologies and multi-target interactions will be key to scaling this approach.

**Contact-point assumptions.** The policy implicitly assumes that the robot can access and apply force near the central stem. In practice, dense foliage, geometric constraints, or safety concerns may prevent ideal contact. Although we mitigate risk with carefully tuned torque, velocity, and joint constraints, these parameters are specific to our hardware and may require adaptation for other platforms. Future work could incorporate contact-aware planning, tactile sensing, or learned strategies for safer and more adaptive interaction in constrained spaces.

**Residual sim-to-real gap.** Despite domain randomization over depth noise and physical properties, some discrepancies persist. Sensor artifacts, lighting changes (e.g., outdoor sunlight), and unmodeled plant dynamics (e.g., wind or high-frequency leaf motion) can impact transfer fidelity. Enhancing perception robustness-through real-to-sim adaptation, or more invariant visual encoders-could improve generalization under broader real-world conditions.

Our policy was trained using an abstract plant model without a photorealistic digital twin. While this morphology-based approach proved sufficient for generalization to stemmed plants, we do not claim that accurate reconstruction is unnecessary. In fact, incorporating detailed digital twins could improve performance in edge cases by providing more precise visual and mechanical cues. Exploring this trade-off between abstraction and realism remains a promising direction.

Despite these limitations, our results mark a significant step toward robust, vision-based manipulation in unstructured, deformable environments. Future efforts should target broader plant morphologies (e.g., vines, creepers), richer occlusion scenarios, and increased autonomy under field conditions-ultimately enabling agricultural robots to operate reliably in complex, real-world crop settings.

## Acknowledgments

This work is jointly funded from NSF-USDA COALESCE grant #2021-67021-34418 and AIIRA grant #2021-67021-35329

## References

- [1] Z. Zerun, T. Xiaowei, C. Chen, P. Fangyu, Y. Rong, Z. Lin, L. Zepeng, and W. Jiawei. High precision and efficiency robotic milling of complex parts: Challenges, approaches and trends. *Chinese Journal of Aeronautics*, 35(2):22–46, 2022.
- [2] Z. Liu, Q. Liu, W. Xu, L. Wang, and Z. Zhou. Robot learning towards smart robotic manufacturing: A review. *Robotics and Computer-Integrated Manufacturing*, 77:102360, 2022.
- [3] P. Bilancia, J. Schmidt, R. Raffaelli, M. Peruzzini, and M. Pellicciari. An overview of industrial robots control and programming approaches. *Applied Sciences*, 13(4):2582, 2023.
- [4] A. Angelopoulos, J. F. Cahoon, and R. Alterovitz. Transforming science labs into automated factories of discovery. *Science Robotics*, 9(95):eadm6991, 2024. doi:10.1126/scirobotics.adm6991. URL <https://www.science.org/doi/abs/10.1126/scirobotics.adm6991>.
- [5] J. Boyd. Robotic laboratory automation. *Science*, 295(5554):517–518, 2002. doi:10.1126/science.295.5554.517. URL <https://www.science.org/doi/abs/10.1126/science.295.5554.517>.
- [6] J. Jacob, S. Cai, P. V. K. Borges, T. Bandyopadhyay, and F. Ramos. Gentle manipulation of tree branches: A contact-aware policy learning approach. In *8th Annual Conference on Robot Learning*.
- [7] M. Rijal, R. Shrestha, T. Smith, and Y. Gu. Force aware branch manipulation to assist agricultural tasks, 2025. URL <https://arxiv.org/abs/2503.07497>.
- [8] J. Jun, J. Kim, J. Seol, J. Kim, and H. I. Son. Towards an efficient tomato harvesting robot: 3d perception, manipulation, and end-effector. *IEEE access*, 9:17631–17640, 2021.
- [9] B. Arad, J. Balendonck, R. Barth, O. Ben-Shahar, Y. Edan, T. Hellström, J. Hemming, P. Kurtser, O. Ringdahl, T. Tielen, et al. Development of a sweet pepper harvesting robot. *Journal of field robotics*, 37(6):1027–1039, 2020.
- [10] C. Chi, B. Burchfiel, E. Cousineau, S. Feng, and S. Song. Iterative residual policy: for goal-conditioned dynamic manipulation of deformable objects. *The International Journal of Robotics Research*, 43(4):389–404, 2024.
- [11] A. Nair, D. Chen, P. Agrawal, P. Isola, P. Abbeel, J. Malik, and S. Levine. Combining self-supervised learning and imitation for vision-based rope manipulation. In *2017 IEEE international conference on robotics and automation (ICRA)*, pages 2146–2153. IEEE, 2017.
- [12] J. Luo, C. Xu, X. Geng, G. Feng, K. Fang, L. Tan, S. Schaal, and S. Levine. Multistage cable routing through hierarchical imitation learning. *IEEE Transactions on Robotics*, 40:1476–1491, 2024. doi:10.1109/TRO.2024.3353075.
- [13] H. Ha and S. Song. Flingbot: The unreasonable effectiveness of dynamic manipulation for cloth unfolding. In *Conference on Robot Learning*, pages 24–33. PMLR, 2022.
- [14] Z. Huang, X. Lin, and D. Held. Mesh-based dynamics with occlusion reasoning for cloth manipulation. *arXiv preprint arXiv:2206.02881*, 2022.

- [15] X. Lin, Y. Wang, J. Olkin, and D. Held. Softgym: Benchmarking deep reinforcement learning for deformable object manipulation. In *Conference on Robot Learning*, pages 432–448. PMLR, 2021.
- [16] T. Boroushaki, J. Leng, I. Clester, A. Rodriguez, and F. Adib. Robotic grasping of fully-occluded objects using rf perception. In *2021 IEEE International Conference on Robotics and Automation (ICRA)*, pages 923–929. IEEE, 2021.
- [17] P. M. Scheickl, N. Schreiber, C. Haas, N. Freymuth, G. Neumann, R. Lioutikov, and F. Mathis-Ullrich. Movement primitive diffusion: Learning gentle robotic manipulation of deformable objects. *IEEE Robotics and Automation Letters*, 9(6):5338–5345, 2024. doi:10.1109/LRA.2024.3382529.
- [18] S. Yao, S. Pan, M. Bennewitz, and K. Hauser. Safe leaf manipulation for accurate shape and pose estimation of occluded fruits, 2025. URL <https://arxiv.org/abs/2409.17389>.
- [19] S. Yao and K. Hauser. Estimating tactile models of heterogeneous deformable objects in real time. In *2023 IEEE International Conference on Robotics and Automation (ICRA)*, pages 12583–12589, 2023. doi:10.1109/ICRA48891.2023.10160731.
- [20] X. Zhang and S. Gupta. Push past green: Learning to look behind plant foliage by moving it, 2024. URL <https://arxiv.org/abs/2307.03175>.
- [21] C. H. Kim, M. Lee, O. Kroemer, and G. Kantor. Towards robotic tree manipulation: Leveraging graph representations. In *2024 IEEE International Conference on Robotics and Automation (ICRA)*, pages 11884–11890, 2024. doi:10.1109/ICRA57147.2024.10611327.
- [22] J. Jacob, S. Cai, P. V. K. Borges, T. Bandyopadhyay, and F. Ramos. Gentle manipulation of tree branches: A contact-aware policy learning approach. In P. Agrawal, O. Kroemer, and W. Burgard, editors, *Proceedings of The 8th Conference on Robot Learning*, volume 270 of *Proceedings of Machine Learning Research*, pages 631–648. PMLR, 06–09 Nov 2025. URL <https://proceedings.mlr.press/v270/jacob25a.html>.
- [23] C. Schuetz, J. Baur, J. Pfaff, T. Buschmann, and H. Ulbrich. Evaluation of a direct optimization method for trajectory planning of a 9-dof redundant fruit-picking manipulator. In *2015 IEEE International Conference on Robotics and Automation (ICRA)*, pages 2660–2666, 2015. doi:10.1109/ICRA.2015.7139558.
- [24] A. Tafuro, B. Debnath, A. M. Zanchettin, and A. G. E. dpmp-deep probabilistic motion planning: A use case in strawberry picking robot, 2022. URL <https://arxiv.org/abs/2208.09074>.
- [25] T. Parhar, H. Baweja, M. Jenkins, and G. Kantor. A deep learning-based stalk grasping pipeline. In *2018 IEEE International Conference on Robotics and Automation (ICRA)*, pages 6161–6167. IEEE, 2018.
- [26] M. Jenkins and G. Kantor. Online detection of occluded plant stalks for manipulation. In *2017 IEEE/RSJ International Conference on Intelligent Robots and Systems (IROS)*, pages 5162–5167. IEEE, 2017.
- [27] L. Luo, H. Wen, Q. Lu, H. Huang, W. Chen, X. Zou, and C. Wang. Collision-free path-planning for six-dof serial harvesting robot based on energy optimal and artificial potential field. *Complexity*, 2018(1):3563846, 2018. doi:<https://doi.org/10.1155/2018/3563846>. URL <https://onlinelibrary.wiley.com/doi/abs/10.1155/2018/3563846>.
- [28] J. Kwon, L. Yang, R. Nowak, and J. Hanna. An empirical study on the power of future prediction in partially observable environments, 2025. URL <https://arxiv.org/abs/2402.07102>.

- [29] R. T. Icarte, R. Valenzano, T. Q. Klassen, P. Christoffersen, A. massoud Farahmand, and S. A. McIlraith. The act of remembering: a study in partially observable reinforcement learning, 2020. URL <https://arxiv.org/abs/2010.01753>.
- [30] Q. Liu, A. Chung, C. Szepesvári, and C. Jin. When is partially observable reinforcement learning not scary?, 2022. URL <https://arxiv.org/abs/2204.08967>.
- [31] J. Matas, S. James, and A. J. Davison. Sim-to-real reinforcement learning for deformable object manipulation, 2018. URL <https://arxiv.org/abs/1806.07851>.
- [32] S. Höfer, K. Bekris, A. Handa, J. C. Gamboa, M. Mozifian, F. Golemo, C. Atkeson, D. Fox, K. Goldberg, J. Leonard, C. Karen Liu, J. Peters, S. Song, P. Welinder, and M. White. Sim2real in robotics and automation: Applications and challenges. *IEEE Transactions on Automation Science and Engineering*, 18(2):398–400, 2021. doi:10.1109/TASE.2021.3064065.
- [33] P. M. Scheikl, E. Tagliabue, B. Gyenes, M. Wagner, D. Dall’Alba, P. Fiorini, and F. Mathis-Ullrich. Sim-to-real transfer for visual reinforcement learning of deformable object manipulation for robot-assisted surgery. *IEEE Robotics and Automation Letters*, 8(2):560–567, 2023. doi:10.1109/LRA.2022.3227873.
- [34] M. Mittal, C. Yu, Q. Yu, J. Liu, N. Rudin, D. Hoeller, J. L. Yuan, R. Singh, Y. Guo, H. Mazhar, A. Mandlekar, B. Babich, G. State, M. Hutter, and A. Garg. Orbit: A unified simulation framework for interactive robot learning environments. *IEEE Robotics and Automation Letters*, 8(6):3740–3747, 2023. doi:10.1109/LRA.2023.3270034.
- [35] J. Schulman, F. Wolski, P. Dhariwal, A. Radford, and O. Klimov. Proximal policy optimization algorithms. *arXiv preprint arXiv:1707.06347*, 2017.
- [36] A. Serrano-Muñoz, D. Chrysostomou, S. Bøgh, and N. Arana-Arexolaleiba. skrl: Modular and flexible library for reinforcement learning. *Journal of Machine Learning Research*, 24(254): 1–9, 2023. URL <http://jmlr.org/papers/v24/23-0112.html>.
- [37] L. Keselman, J. Iselin Woodfill, A. Grunnet-Jepsen, and A. Bhowmik. Intel realsense stereoscopic depth cameras. In *Proceedings of the IEEE conference on computer vision and pattern recognition workshops*, pages 1–10, 2017.

## 8 Appendix

### Training Configuration

```
models:
  policy and value:
    class: GaussianMixin
    clip_actions: true
    clip_log_std: true
    initial_log_std: 0.0
    network:
      - name: image_features
        input: image
        layers: [conv2d(32,8,4), conv2d(128,4,2), conv2d(128,3,1), conv2d(128,3,1),
                flatten]
        activations: elu
      - name: ee_features
        input: ee_position
        layers: [64, 64]; activations: elu
      - name: joint_features
        input: joints
        layers: [64, 64]; activations: elu
      - name: combined
        input: concatenate([image_features, ee_features, joint_features])
        layers: [512]; activations: elu
        output: ACTIONS and ONE for policy and value respectively

agent:
  class: PPO
  rollouts: 32; learning_epochs: 5; mini_batches: 32
  discount_factor: 0.99; lambda: 0.95
  learning_rate: 3e-4
  learning_rate_scheduler: KLAdaptiveLR
  learning_rate_scheduler_kwargs: {kl_threshold: 0.008}

preprocessors:
  state: RunningStandardScaler (obs space)
  value: RunningStandardScaler (scalar)
```

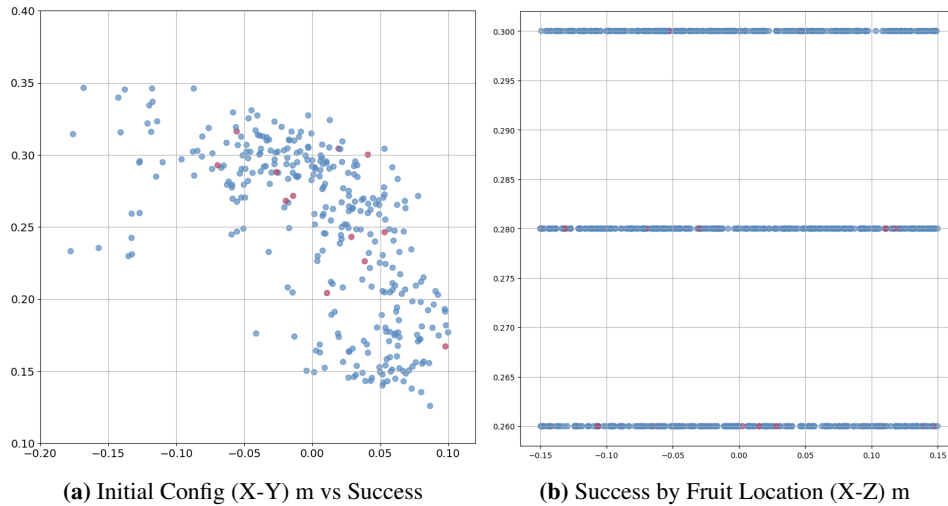
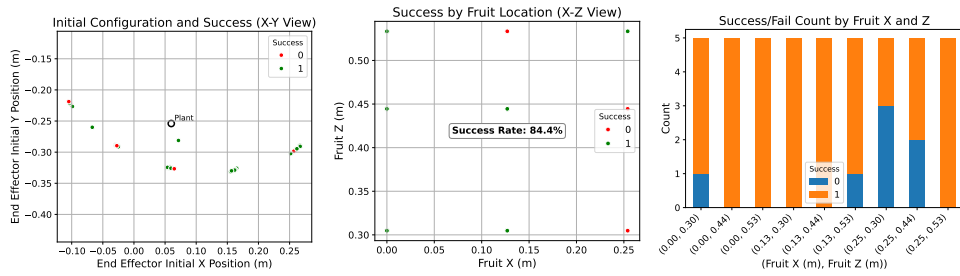
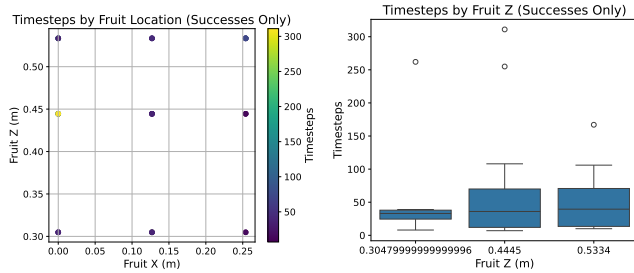


**Figure 6:** Simulation Results. Red denotes failure and blue denotes success

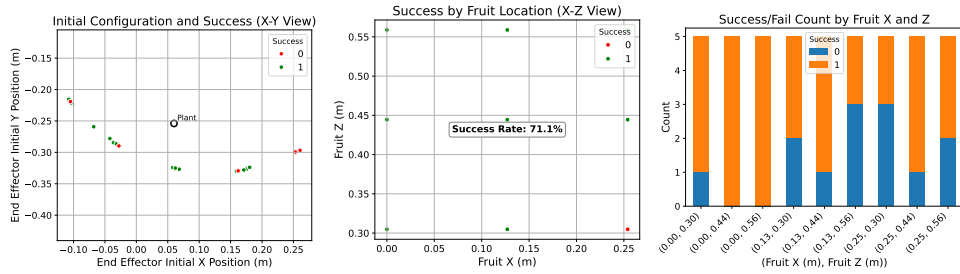


(a) Initial Config Success (b) Success by Fruit Location (c) Success/Fail by Fruit XZ

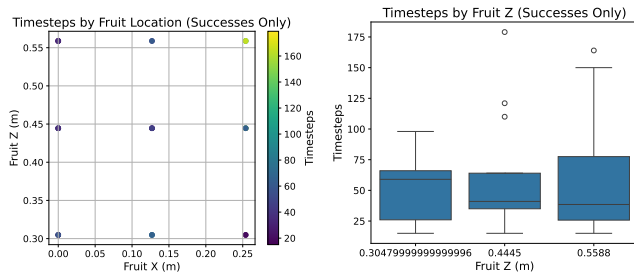


(d) Timesteps by Fruit Location (e) Timesteps by Fruit Z

Figure 7: Evaluation results for plant I

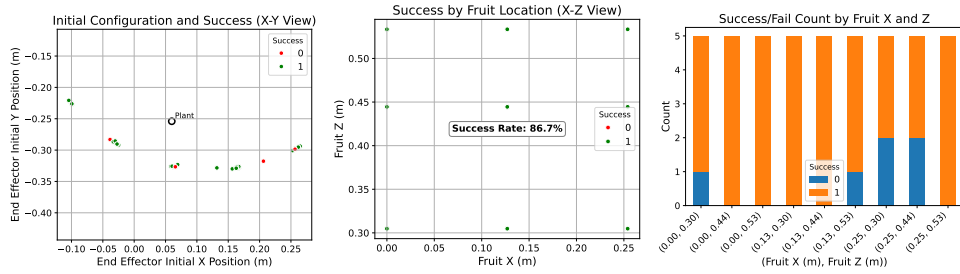


(a) Initial Config Success (b) Success by Fruit Location (c) Success/Fail by Fruit XZ

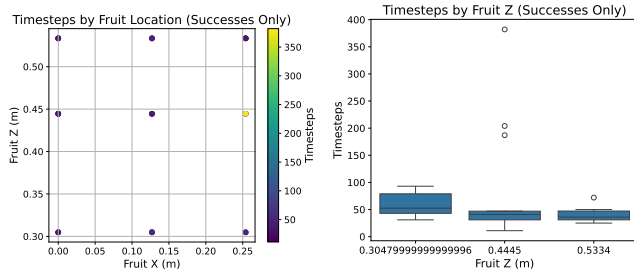


(d) Timesteps by Fruit Location (e) Timesteps by Fruit Z

Figure 8: Evaluation results for plant II

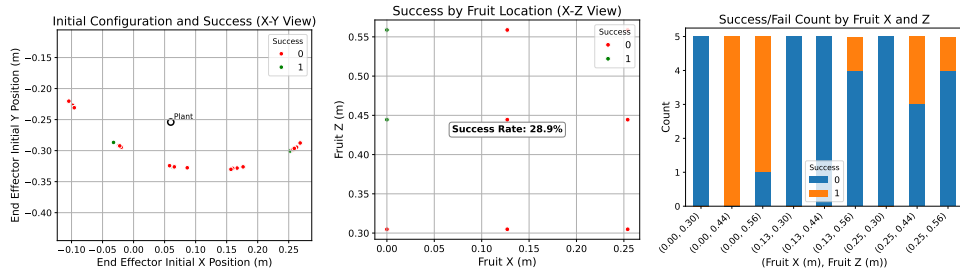


(a) Initial Config Success (b) Success by Fruit Location (c) Success/Fail by Fruit XZ

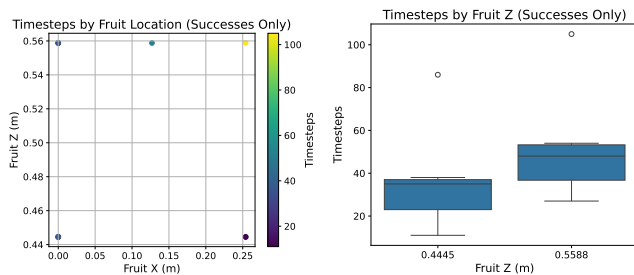


(d) Timesteps by Fruit Location (e) Timesteps by Fruit Z

Figure 9: Evaluation results for Plant III



(a) Initial Config Success (b) Success by Fruit Location (c) Success/Fail by Fruit XZ



(d) Timesteps by Fruit Location (e) Timesteps by Fruit Z

Figure 10: Evaluation results for Plant IV

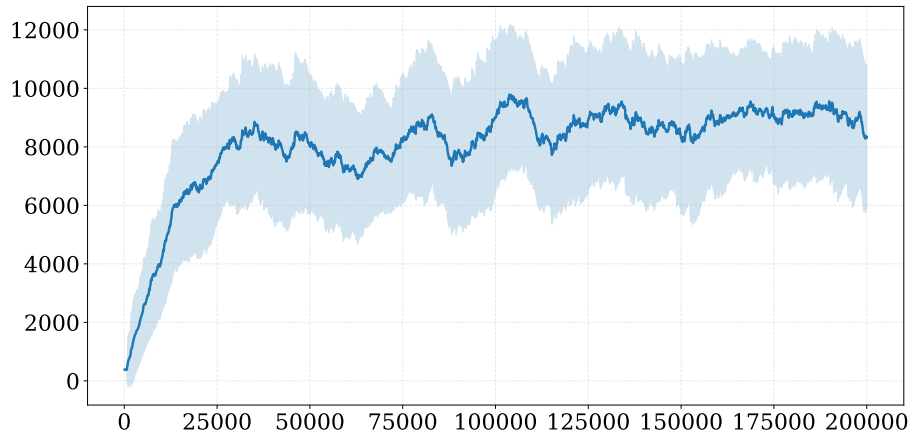
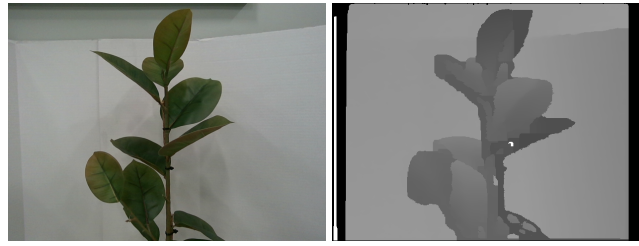


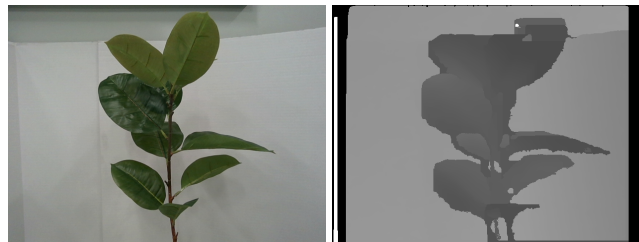
**Figure 11:** Reward Plot of Low Fidelity Training in the Simulation. The X-axis is the timesteps per environment, with 64 environments



(a) RGB

(b) Depth

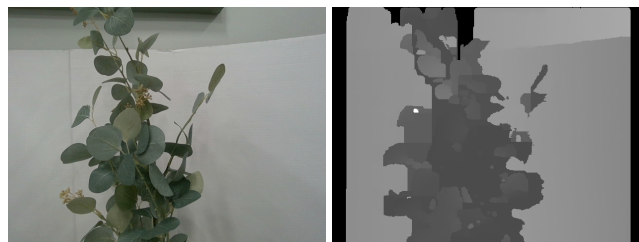
**Figure 12:** Plant I RGB and Depth Images



(a) RGB

(b) Depth

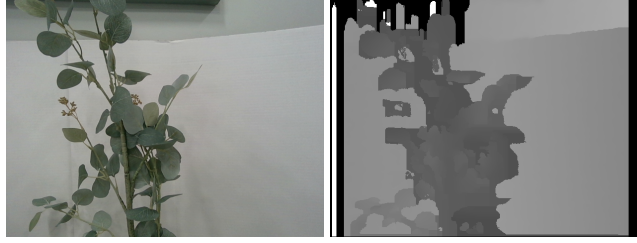
**Figure 13:** Plant II RGB and Depth Images



(a) RGB

(b) Depth

**Figure 14:** Plant IV RGB and Depth Images



(a) RGB (b) Plant

Figure 15: Plant V RGB and Depth Images

Initial Conf X-Y (m)	Fruit Loc X-Z (m)				
	(-0.10,-0.22)	(-0.02,-0.29)	(0.07,-0.33)	(0.17,-0.33)	(0.26,-0.30)
(0.00,0.30)	1	1	1	1	0
(0.00,0.44)	1	1	1	1	1
(0.00,0.53)	1	1	1	1	1
(0.13,0.30)	1	1	1	1	1
(0.13,0.44)	1	1	1	1	1
(0.13,0.53)	0	1	1	1	1
(0.25,0.30)	0	0	0	1	1
(0.25,0.44)	0	1	0	1	1
(0.25,0.53)	1	1	1	1	1

Table 2: Table showing the number of successful trials for plant I across various Initial End Effector Positions with Fruit Location.

Initial Conf X-Y (m)	Fruit Loc X-Z (m)				
	(-0.10,-0.22)	(-0.02,-0.29)	(0.07,-0.33)	(0.17,-0.33)	(0.26,-0.30)
(0.00,0.30)	1	1	1	1	0
(0.00,0.44)	1	1	1	1	1
(0.00,0.53)	1	1	1	1	1
(0.13,0.30)	1	1	1	0	0
(0.13,0.44)	1	1	1	0	1
(0.13,0.53)	0	1	1	0	0
(0.25,0.30)	1	0	0	1	0
(0.25,0.44)	0	1	1	1	1
(0.25,0.53)	0	1	1	1	0

Table 3: Table showing the number of successful trials for plant II across various Initial End Effector Positions with Fruit Location.

Initial Conf X-Y (m)	Fruit Loc X-Z (m)				
	(-0.10,-0.22)	(-0.02,-0.29)	(0.07,-0.33)	(0.17,-0.33)	(0.26,-0.30)
(0.00,0.30)	1	1	1	0	1
(0.00,0.44)	1	1	1	1	1
(0.00,0.53)	1	1	1	1	1
(0.13,0.30)	1	1	1	1	1
(0.13,0.44)	1	1	1	1	1
(0.13,0.53)	1	0	1	1	1
(0.25,0.30)	1	0	1	1	0
(0.25,0.44)	1	0	0	1	1
(0.25,0.53)	1	1	1	1	1

Table 4: Table showing the number of successful trials for Plant III across various Initial End Effector Positions with Fruit Location.

Initial Conf X-Y (m)	Fruit Loc X-Z (m)				
	(-0.10,-0.22)	(-0.02,-0.29)	(0.07,-0.33)	(0.17,-0.33)	(0.26,-0.30)
(0.00,0.30)	0	0	0	0	0
(0.00,0.44)	1	1	1	1	1
(0.00,0.53)	1	1	1	0	1
(0.13,0.30)	0	0	0	0	0
(0.13,0.44)	0	0	0	0	0
(0.13,0.53)	0	0	1	0	0
(0.25,0.30)	0	0	0	0	0
(0.25,0.44)	0	0	1	0	1
(0.25,0.53)	0	0	0	0	1

**Table 5:** Table showing the number of successful trials for Plant IV across various Initial End Effector Positions with Fruit Location.